Atmos. Meas. Tech. Discuss., https://doi.org/10.5194/amt-2019-121
Manuscript under review for journal Atmos. Meas. Tech.
Discussion started: 28 March 2019

Atmospheric Measurement Techniques Discussions

Ground-based measurements of middle-atmospheric carbon monoxide above Ny-Ålesund (78.9° N, 11.9° E)

Niall J. Ryan[1], Mathias Palm[1], Christoph G. Hoffmann[2], Jens Goliasch[3], Justus Notholt[1]

[1]Institute of Environmental Physics, University of Bremen, Bremen, 28359, Germany
[2]Institute of Physics, University of Greifswald, Felix-Hausdorff-Str. 6, 17489, Greifswald, Germany
[3]RPG-Radiometer Physics GmbH, Werner-von-Siemens-Str. 4, 53340 Meckenheim, Germany

Correspondence to: Niall J. Ryan (n_ryan@iup.physik.uni-bremen.de)

Abstract. We present a new ground-based system for measurements of middle-atmospheric carbon monoxide (CO) at Ny-Ålesund, Svalbard, and the altitude profiles of CO volume mixing ratios (VMR) measured during the 2017/2018 winter. The Carbon Monoxide Radiometer for Atmospheric Measurements (CORAM) records spectra from CO emissions in the middle-atmosphere with the aid of a low-noise amplifier designed for the 230 GHz spectral region. Altitude profiles of CO VMRs are retrieved from the measured spectra using an optimal estimation inversion technique. The profiles in the current dataset have an average altitude range of 47-87 km and an estimated precision peaking at ~ 12 % of the a priori used in the inversion. The CORAM profiles are compared to collocated CO measurements from the Microwave Limb Sounder (MLS) aboard the Aura satellite and show a difference of 7.4 – 16.1 %, with a maximum absolute difference of 2.5 ppmv at 86 km altitude. CO profiles are currently available at 1 hr resolution between November 2017 and January 2018.

1 Introduction

Radiometers are powerful tools for measuring the composition of the atmosphere. This is particularly true for areas where there are prolonged night-time periods, such as the poles. Radiometers can measure emissions from molecules in the atmosphere, thus removing any reliance on the sun. Electronic manipulation of the measured atmospheric signal makes it possible to detect signals with very low intensities, especially when the electronics are cooled to low temperatures, thus producing lower thermal noise.

Altitude profiles of carbon monoxide (CO) concentrations in the middle atmosphere are useful in quantifying dynamical processes. Because the lifetime of CO during polar night is on the order of months (Solomon et al., 1985; Allen et al., 1999), it is a good tracer for atmospheric dynamics. The generally increasing volume mixing ratio (VMR) of CO with altitude has a strong gradient, which helps to identify the origin of increases or decreases in concentration. An example of this is during polar night when CO concentrations increase in the middle atmosphere due to the vertical branch of the residual mean circulation bringing CO-rich air from higher altitudes (Smith et al., 2011; Garcia et al., 2014). Similarly, a decrease in middle-atmospheric CO in polar spring is linked to a change in direction of the residual mean circulation at this time. The breakup of the polar vortex in spring also allows for more CO-poor air to be transported poleward from lower latitudes

(Manney et al., 2009; 2015), adding complexity to the quantitative link between dynamical processes and variations in CO. Changes in CO (and other tracers) VMRs can be caused by chemical production/loss (night-time CO is lost through reaction with a layer of hydroxyl at ~ 82 km (Solomon et al., 1985; Brinksma et al., 1998; Damiani et al., 2010; Ryan et al., 2018), and by dynamical processes: vertical/horizontal advection, eddy transport, and to a lesser extent, molecular diffusion (Garcia and Solomon, 1983; Andrews et al., 1987, Brasseur and Solomon, 2005; Smith et al., 2011). While vertical advection is, in general, the dominating process, modelling studies of middle-atmospheric CO indicate that the vertical transport rates calculated from trace gas measurements do not accurately represent the mean descent/ascent of the atmosphere because the 'true' effect of vertical advection is masked by other processes (Hoffmann, 2012; Ryan et al., 2018).

The general increase in middle-atmospheric CO VMR during polar night is seen in multiple datasets (e.g., Allen et al., 2000, Forkman et al., 2005, Funke et al., 2009, Hoffmann et al., 2011, Ryan et al 2017), and the phenomenon has been observed for other tracers, e.g., H_2O (Lee et al., 2011; Straub et al., 2012), N_2O, CH_4, and H_2O (Nassar et al., 2005), and NO, CH_4, and H_2O (Bailey et al., 2014). The calculated rates of vertical tracer transport in the above studies range from -1200 to +450 m/day (negative numbers indicate descent), with the values representing varying averages in space and/or time. Variations in tracer VMRs on smaller timescales (minutes to hours) can be caused by waves that displace air parcels from their equilibrium positions and perturb trace gas profiles (e.g. Zhu and Holton, 1997; Ekermann et al., 1998; Fritts and Alexander, 2003; Noguchi et al., 2006; Chane Ming et al., 2016). Data from ground-based radiometers with relatively high time resolution have be used to investigate small periodic fluctuations in ozone (O_3) and water vapour (Hocke et al., 2006; Moreira et al., 2018, Schranz et al., 2018). The positive gradient of polar CO VMRs with altitude throughout the middle atmosphere, coupled with the time resolution of the presented measurement system at Ny-Ålesund (≤ 1 hr), means that the dataset discussed here is well-suited to observing these periodic fluctuations, which are likely to be caused by vertical advection of air parcels by gravity waves (Zhu and Holton, 1997; Ekermann et al., 1998; Hocke et al., 2006). The Kiruna Microwave Radiometer, KIMRA, is also currently making measurements of middle-atmospheric CO at 67.8° N (Raffalski et al, 2005; Hoffmann et al., 2011; Ryan et al., 2017), and the addition of a new instrument at Ny-Ålesund provides a needed increase in Arctic coverage and an excellent opportunity for comparison of CO at locations near the polar vortex edge and inside the vortex, particularly during dynamic events such as sudden stratospheric warmings (SSWs).

The high time resolution of the CO Radiometer for Atmospheric Measurements (CORAM) is achieved primarily with a high-frequency low-noise amplifier (LNA), which operates on the atmospheric CO signal at 230.54 GHz before the signal is mixed with the radiometer's local oscillator. CORAM is discussed in Section 2, as well as the inversion method, CO profile characteristics, and error estimates. Section 3 shows the results of a comparison with collocated data from the Microwave Limb Sounder (MLS). Section 4 shows the CORAM profile timeseries and discusses the usage of the data, and Section 5 offers some concluding remarks.

Atmos. Meas. Tech. Discuss., https://doi.org/10.5194/amt-2019-121
Manuscript under review for journal Atmos. Meas. Tech.
Discussion started: 28 March 2019

2 Instrument and measured data

2.1 CORAM

CORAM is housed at Ny-Ålesund, Svalbard (78.9° N, 11.9° E), and is part of the joint French-German Arctic Research Base, AWIPEV. CORAM measures the J = 2 → 1 rotational transition of CO at 230.54 GHz. The instrument was installed in 2017 and made first measurements of CO in the winter of 2017/2018. The atmospheric signal enters the lab at 20° elevation and is directed by a series of mirrors through a window in a cryocooler, fed into a corrugated horn antenna and amplified by a 230 GHz LNA. The unwanted sideband at ~ 213.5 GHz is supressed with a waveguide filter before the atmospheric signal is mixed with the local oscillator (LO) signal (111 GHz) using a sub-harmonic mixer. Now at an intermediate frequency of 8.5 GHz, the signal exits the cooler and is amplified with another LNA before being further downconverted to 1.5 GHz and analysed by a Fast Fourier Transform Spectrometer (FFTS). Figure 1 shows a schematic drawing of the receiver including the components in the cryocooler. Figure 2a shows the frequency response of the waveguide filter with a suppression of ~ -45 dB at 213.5 GHz.

Each electronic component in a signal chain will add noise to the atmospheric signal of interest, which will also be amplified with any subsequent amplifiers. Because of the greater availability/cost/quality of amplifiers that operated at several GHz, radiometers used for atmospheric measurements have generally employed LNAs after the atmospheric signal has been mixed with the LO and has been downconverted to a lower frequency. The first LNA in CORAM, produced by Radiometer Physics GmbH (RPG), operates at a relatively high frequency of 230 GHz and allows for the atmospheric signal to be amplified before it encounters the mixer, ultimately providing an increased signal-to-noise ratio (SNR) for an atmospheric measurement. Figure 2b shows the receiver noise temperature (Janssen, 1993) for CORAM measured at the exit of the cryocooler, with the cryocooler components at a typical temperature of 39 K. At 8.5 GHz, the receiver noise temperature is below 350 K. The measurement time needed to produce a spectrum with a desired SNR is proportional to the square of the system noise temperature, which also includes contributions from the second downconversion, the atmospheric background and signal, and quasioptical spillover (Parrish et al., 1988, Janssen, 1993, Stanimirović et al., 2002). The single sideband system noise temperature of CORAM is ~ 600 K.

The measured signal is calibrated using two blackbody targets at known temperatures: a cold target in the cryocooler at ~ 70 K and a warm target at ~ 293 K. A path length modulator is part of the setup that directs the atmospheric signal to the feedhorn, in order to reduce the amplitude of any standing waves in the quasioptics. The FFTS is an Acqiris AC240 and has a bandwidth of 1 GHz with 16384 channels. The atmospheric measurements are all made with an elevation angle of 20° and so the individually recorded spectra can be averaged together to reduce the SNR. The measurements used here have been spectrally averaged over approximately 1 hour, including time used to calibrate the signal. Finer time resolutions that still yield usefully high SNRs are possible.

Atmos. Meas. Tech. Discuss., https://doi.org/10.5194/amt-2019-121
Manuscript under review for journal Atmos. Meas. Tech.
Discussion started: 28 March 2019

2.2 Inversion method

Altitude profiles of CO VMR are retrieved from the measured spectra using an optimal estimation inversion technique (Rodgers, 2000). The method uses some a priori information of the state of the atmosphere to constrain the profile that is retrieved from the measured spectrum. The inversions are performed with the Qpack2 package (Eriksson et al., 2005), which uses the Atmospheric Radiative Transfer Simulator (ARTS 2, Eriksson et al., 2011) to model the transfer of radiation through the earth's atmosphere. The a priori CO profile used in the inversion is the average of one winter (September through April) of output from WACCM4 (Garcia et al., 2007), provided by Douglas Kinnison at the National Centre for atmospheric research (NCAR). The output is on a 132-layer grid between approximately ground and 130 km altitude. A standard deviation of 100% at all altitudes was found to provide enough freedom for expected changes in CO VMR to be captured by the inversion, and to give enough regularisation of the solution. Oscillations in the CO profile, a sign of over-fitting to the measurement (Rodgers, 2000), were found in several profiles. The oscillations were large in these cases so the CO profiles were considered unphysical and rejected. CO emissions are attenuated by water vapour in the atmosphere and this is accounted for by including the water vapour continuum by Rosenkranz (1998) in the forward model and inversion. O_3 is also simultaneously retrieved with CO, as an O_3 spectral line lies at 231.28 GHz. The molecular oxygen (O_2) and nitrogen (N_2) continua (Rosenkranz, 1993), as well as nitric acid (HNO_3) spectral lines, are included in the inversion but are not retrieved and are considered model parameters. The spectroscopic line data used here is from the high resolution transmission molecular absorption database (HITRAN) 2008 catalogue (Rothmann et al., 2009). The a priori information for O_2 and O_3, and water vapour is from the same WACCM4 run as for CO, and the information for HNO_3 and N_2 are from the FASCOD (Fast Atmospheric Signature Code) subarctic winter scenario (Anderson et al., 1986).

The information for the altitude, pressure, and temperature in an inversion is constructed from European Centre for Medium-Range Weather Forecasting (ECMWF) profiles and from the NRLMSISE-00 empirical model of the atmosphere (MSIS from herein) (Picone et al., 2002). ECMWF information is available four times per day and covers up to 0.01 hPa altitude, and above that the temperature profile information is from MSIS. The temperature data is smoothed around the point where the profiles are merged to avoid discontinuities.

An estimate of the measurement noise on a spectrum is made by fitting a second-order polynomial to a wing of the spectrum and calculating the standard deviation of the fit. Qpack2 provides the capability to fit a series of functions to the baseline of the measured spectra (a baseline fit) to account for errors in the baseline which are likely caused by standing waves in the instrument. The baseline fit is included in the optimal estimation and forms part of the overall fit to the measurement (inversion fit). All of the CORAM measured spectra were first inverted without a fit to the baseline and a periodogram of the residuals was evaluated to determine the periods of sinusoidal signatures in the baseline. Three primary sinusoids were found to be present, with respective estimated periods of 125, 62.5, and 41.67 MHz, and amplitudes of 0.2, 0.1, and 0.02 K. The periods of the sinewaves are large compared with the width of the CO spectral line and so are uniquely distinguishable from

it. A first order polynomial is also included in the baseline fit to account for offsets. The zeroth- and first-order coefficients have estimated uncertainties of 1 and 0.5 K respectively.

The altitude grid for the forward model is between the ground and 125 km, with approximately equally-spaced points. The retrieval grid is between approximately 2 and 124 km, and is a 62-layer subset of the forward model grid. CO VMRs are retrieved as a fraction of the a priori for numerical stability due the strong gradients in atmospheric CO. The inversion method is nonlinear and uses a Marquardt–Levenberg iterative minimisation scheme (Marquardt, 1963).

2.3 CO profile characteristics

The CORAM CO data spans November 18th 2017 to January 18th 2018. The instrument required maintenance after this date and was not in full operation for the remainder of the winter, unfortunately missing the SSW in February ☹. Nonetheless, the data shown here consists of 875 atmospheric profiles in that time, with time resolution of ~ 1 hr.

Figure 3 shows an example spectrum measured by CORAM on December 24th 2017, and the matching inversion fit and residual. The retrieved CO profile is also plotted in Fig. 3 alongside the a priori profile. The mean of the averaging kernels for the whole CO data set are shown in Fig. 4 alongside the average of the estimated altitude resolution of the CO profiles. The averaging kernels describe the sensitivity of a retrieved CO VMR at a given altitude, to CO at other altitudes (Rodgers, 2000). The estimated altitude resolution of the profiles is calculated here as the full-width at half-maximum (FWHM) of the averaging kernels. A common way to estimate the altitude limits of a retrieved profile is to define the sum of the rows of the averaging kernels as the measurement response and assign a cut-off value. The choice of the cut-off value is rather arbitrary but 0.8 is regularly used (e.g., Forkmann et al., 2012; Straub et al., 2013, Schranz et al., 2018), and is also used here. With the above definitions, the CO profiles from CORAM during winter 2017/2018 have an average altitude range of approximately 47 – 87 km, with an average altitude resolution varying between approximately 12.5 and 28 km over that range. The retrieval range can change depending on the distribution of CO in the atmosphere (the lower limit can decrease in altitude when there are higher CO values at lower altitudes) and the value provided here is the mean range over the time span of the data.

The retrieval limits will vary from measurement to measurement and individual profiles should be considered in combination with the accompanying averaging kernels. The centres of the averaging kernels, when represented in VMR, are shifted down in altitude compared to a representation in relative units (Hoffmann et al., 2011). The lower limit of the retrieval here is defined by the SNR in the measurement and the upper limit is set by a transition from a pressure broadening regime to a doppler broadening one. The result of this change is that, above approximately 70 km in the VMR representation, the centres of the averaging kernels do not increase in altitude with their corresponding retrieval altitudes. The retrieved CO values above ~ 70 km altitude do contain information from the atmosphere that corresponds with the retrieval altitude, but the VMR representation of the profile should be considered with care. Hoffmann et al. (2011) provides a detailed discussion on the representation of data for ground-based CO measurements.

Atmos. Meas. Tech. Discuss., https://doi.org/10.5194/amt-2019-121
Manuscript under review for journal Atmos. Meas. Tech.
Discussion started: 28 March 2019

2.4 CO profile error estimates

The error contributions to the CO profiles are calculated using OEM error definitions, which are defined in detail in Rodgers (2000). The estimates of the errors are found by perturbing the inputs to the inversion, using the following uncertainties. Error in the temperature profile is the same as that used in Hoffmann (2011): 10% above 100 km, 5% below 80 km, and linearly interpolated in between. An uncertainty of 1° is chosen for the pointing of the instrument to the sky, an overestimate of the motor uncertainty by an order of magnitude, to account for uncertainties in the orientation of the instrument table. The uncertainty in the warm and cold calibration targets is 2 K, an overestimate that accounts for variations and drifts in the temperatures. The HITRAN 2008 catalogue is used for uncertainties in the CO line parameters: 1% for the line intensity, 2% for the air broadening parameter and 5% for the temperature dependence of the air broadening. The uncertainties related to self-broadening of CO are not considered due to the relatively low concentration of the gas (Ryan and Walker, 2015). The uncertainty in the line position is ignored because the frequency grid used in the inversion can be shifted to centre a measurement.

The error estimates, including the average of the error arising from statistical noise on the spectrum, are plotted in Fig. 5. The sum in quadrature of the error estimates is also plotted, as well as the a priori CO profile for the data set. The statistical noise on the spectrum and the uncertainty in the temperature profile are the biggest contributors to the total error profile, with the temperature error surpassing that of the spectrum noise at ~ 84 km, near the average upper retrieval altitude limit. As a fraction of the a priori profile, the total error estimate has a maximum at ~ 12% at ~ 48 km, near the average lower retrieval altitude limit, and there is also a peak of 11.5% near 70 km altitude. The uncertainty in the temperature profile begins to become more pronounced above 50 km altitude.

3 Comparison with Aura MLS

MLS is a radiometer aboard the Aura satellite. A description of the instrument is given in Waters et al. (2006). Version 4.2 of the MLS CO data (Schwartz et al., 2015) is used here and is described in Livesey et al. (2015). The atmospheric pressure range of the data is 215-0.0046 hPa. The precision of the CO VMR profile reaches a maximum (largest) value of 1.1 ppmv at the upper limit of the MLS CO retrieval altitude. The data has a positive bias in the middle atmosphere, compared to the ACE-FTS satellite instrument, of 20% (Livesey et al., 2015). This bias is estimated from a study of version 2.2 of MLS CO data (Pumphrey et al., 2007), with subsequent versions showing a slight decrease in the CO VMR.

3.1 Colocated measurement comparison

MLS measurements are subset to within ±2° latitude and ±10° longitude of CORAM. The CO VMRs are expected to vary more in latitude than in longitude. A longitude space of ±5° was also tested but there were not significant changes to the results shown here and the number of coincident MLS measurements were halved. Above 0.001 hPa, MLS CO profiles use a

constant VMR value. Because CORAM has some sensitivity to CO at these altitudes, the MLS profiles were instead linearly extrapolated in pressure space above 0.001 hPa. A more physically realistic profile shape is produced, and example of which can be seen in Fig. 4 of Ryan et al. (2017). To reduce the effect of atmospheric variability between individual measurement locations, the CORAM and MLS profiles are averaged by day to produce daily mean profiles. These MLS profiles were smoothed (Rodgers, 2000) with the averaging kernels of the corresponding CORAM profiles to account for the finer altitude resolution of MLS CO profiles: 6-7 km in the upper mesosphere and 3.5 to 5 km in the upper troposphere to the lower mesosphere (Livesey et al., 2015).

Figure 6 shows the mean CO profiles for CORAM and MLS over the time of measurement overlap (mid-November to mid-January), as well as the absolute and percentage (relative to the mean of the MLS and CORAM profiles) differences in the profiles. The correlation of the CO VMRs at each retrieval altitude is also plotted. The maximum absolute difference in the mean profiles is 2.5 ppmv at 86 km altitude, corresponding to an 11.3% difference. The percentage difference varies between ~ 7.4 % at the lowest retrieval altitude and 16.1% at 72 km, with MLS having a low bias in comparison to CORAM over the entire altitude range. This contrasts with the estimated high bias of MLS compared to ACE-FTS, mentioned above. The standard deviation of the differences in the profiles is largest (in percentage) at 58 km with a value of 14.4 %. The correlation of the CO profiles is greater than 0.80 at all retrieval altitudes, reaching a maximum of 0.92 at 47 km. The statistics here show some similarities to the comparison of MLS CO and ground-based CO measurements from KIMRA (67.8° N), where MLS showed a low bias (peaking at ~ 0.65 ppmv) up to ~ 74 km, with a maximum relative bias of 22% at 60 km (Ryan et al., 2017). The correlation between KIMRA and MLS was slightly higher, remaining greater than 0.90 up to 82 km alttiude.

Figure 7 shows the daily time series of the MLS and CORAM profiles at 48, 58, 68, 78, and 88 km. The largest differences in CO are found at higher altitudes (≥ 68 km) in November and the first days of December, after which the values become closer in VMR. The reason for the larger difference over this time is unknown, but it is clear that these high values contribute to the bias between the instruments shown in Fig. 6. Despite the absolute differences, a similar variability in CO is captured by both instruments over the whole time series.

4 CORAM data and usage

Figure 8 shows the currently available CORAM CO data for winter 2017/2018 at 1 hr time resolution. The anomalously high values above ~ 70 km altitude are visible in November and first days of December. At lower altitudes over this time, there is still some downwelling of CO due to the residual mean circulation, before a levelling off in mid-December. A general decrease in middle-atmospheric CO begins around December 22nd, leading to a local minimum in the first week of January. Figure 8 also shows a 43-hour segment of the data beginning at 5 pm on December 31st 2017, to illustrate the advantage of continuous measurements. Below ~75 km altitude, there is apparent downwelling of CO for about the first 25 hours, peaking before VMR values start to decrease over the next 18 hours. There are two relatively strong increases in lower-altitude CO at

approximately 2pm January 1st and 1am January 2nd, evident from the 2.3 ppmv contour line moving down from 60 to 50 km altitude. Over this same time, between 60 and 70 km, there is an oscillation in the 4.1 and 6 ppmv contour lines, with peaks occurring every 1-2 hours. The VMR values above approximately 75 km tend to show similar short-timescale variations but with opposite sign, i.e., a peak at a higher altitude corresponds with a trough at a lower altitude. This inverted pattern is observable over the whole 43-hour time period Variations on these timescales cannot be directly observed by non-geostationary satellites, illustrating the unique capability of ground-based instruments.

These are broad descriptions of the data because one cannot fully characterise the variations in CO without the use of other data sources and model output. Variations on the timescales of an hour to weeks are visible in the data and require detailed study to elucidate the underlying dynamical processes, such as polar vortex shift, Rossby wave activity, SSW events, gravity wave perturbations (time scales of minutes to hours). Peridocities in trace gas data have previously been analysed using spectral decomposition techniques on ground-based measurements of water vapour and ozone (e.g., Struder et al., 2012, Hocke et al., 2013, Schranz et al., 2019) to identify waves with periods of days to weeks.

As mentioned in Sect. 2.3, the CORAM profiles should be used with consideration of the accompanying averaging kernels. Ground-based measurements have limited altitude resolution, often much coarser than the altitude grids onto which the data is retrieved. The representation of the data on a fine grid adds stability to the inversion (Eriksson, 1999) and can give rise to substantial smoothing error in the profiles (Rodgers, 2000). The smoothing error can be accounted for when comparing CORAM to instruments with higher resolution by convolving the data from the other instrument with the CORAM averaging kernels, as was done for MLS in Sect. 3. The error should be assessed if one is to use the CO profiles without considering the sensitivity distribution described by the averaging kernels. This is not a recommended use of the data and why the smoothing error is not assessed in Sect. 2.4. In other words, if one is to say something of a CORAM CO VMR at a given grid point, on must be aware that the VMR value at that grid point contains information from a range of altitudes, with a sensitivity governed by the associated averaging kernel.

CORAM profiles can be used independently to describe changes in CO over time, providing the averaging kernels do not significantly change over this time, which would change the measurement response. In particular, care should be taken at altitudes near the edges of the retrieval range of the profiles, where the measurement response has a strong gradient and can change quickly when there are rapid changes in CO concentrations at those altitudes. CORAM is currently under maintenance due to a fault in the LO signal generator and is expected to be back in operation for the winter of 2019/2020 and beyond.

5 Conclusion

This work presents a new ground-based radiometer, CORAM, that has been installed at the high-Arctic location of Ny-Ålesund, 78.9° N, for the measurement of middle-atmospheric CO. The instrument makes use of a high-frequency LNA, before the downconversion of the atmospheric signal, to achieve high SNRs at time resolutions on the order of an hour or

less. CO profiles were retrieved in the winter of 2017/2018 and error estimates show that the uncertainty in the temperature input for the inversions and the statistical noise on the spectrum are the largest contributions to the error budget, giving a maximum in the error profile of ~ 12 % of the a priori profile. The mean of the averaging kernel matrix for the CORAM dataset gives an average retrieval altitude range of 47-87 km with an average altitude resolution of 12.5 to 28 km over this range. A comparison with MLS shows a negative bias (MLS - CORAM) at all altitudes, with a maximum of 16.1 % of the average profiles occurring at 72 km altitude. A comparison of the instruments' time series indicate abnormally high CO measured by CORAM above ~ 68 km in November that contributes to the observed bias, after which the MLS and CORAM values show improved agreement. Correlations between the instruments range from 0.80 to 0.92 over CORAMs retrievable altitude range. CO profiles above Ny-Ålesund with a 1 hr time resolution between November 2017 to January 2018 are currently available.

Author contribution

M. Palm and C. Hoffmann designed the project. C. Hoffmann, N. Ryan, and J. Goliasch designed and built CORAM. N. Ryan developed the inversion setups for CORAM and performed the comparisons. N. Ryan installed CORAM at Ny-Ålesund, and the instrument was maintained by M. Palm. J. Notholt provided valuable feedback on the project. N. Ryan prepared the manuscript with contributions from co-authors.

Acknowledgements

This work has been funded by the German Federal Ministry of Education and Research (BMBF) through the research project: Role Of the Middle atmosphere in Climate (ROMIC), sub-project: ROMICCO, project number: 01LG1214A, as well as by a grant from the Canadian Space Agency. We would like to express our gratitude to the MLS teams for making their CO product available. We would also like to thank the ECMWF and MSIS teams for making their products available, as well as the Qpack and ARTS communities for making their software available. We thank the AWIPEV staff for all of the help provided at Ny-Ålesund, particularly Benoit Laurent, who aided in the installation and maintenance of CORAM at Ny-Ålesund.

References

Allen, D., Stanford, J., Nakamura, N., López-Valverde, M., López-Puertas, M., Taylor, F., and Remedios, J.: Antarctic polar descent and planetary wave activity observed in ISAMS CO from April to July 1992. Geophys. Res. Lett., 27, 665–668, 2000.

Anderson, G. P., Clough, S. A., Kneizys, F. X., Chetwynd, J. H., and Shettle, E. P.: AFGL atmospheric constituent profiles (0–120 km), Tech. Rep. TR-86-0110, AFGL, 1986.

Bailey, S. M., Thurairajah, B., Randall, C. E., Holt, L., Siskind, D. E., Harvey, V. L., Venkataramani, K., Hervig, M. E., Rong, P., and Russell III, J. M.: A multi tracer analysis of thermo- sphere to stratosphere descent triggered by the 2013 Stratospheric Sudden Warming, Geophys. Res. Lett., 41, 5216–5222, doi:10.1002/2014GL059860, 2014.

Andrews, D., Holton, J., and Leovy, C.: Middle Atmosphere Dynamics, Academic Press, 489 pp., 1987.

Brasseur, G. and Solomon, S.: Aeronomy of the Middle Atmosphere: Chemistry and Physics of the Stratosphere and Mesosphere, Springer, 644 pp., 2005.

Brinksma, E. J., Meijer, Y. J., McDermid, I. S., Cageao, R. P., Bergwerff, J. B., Swart, D. P. J., Ubachs, W., Matthews, W. A., Hogervorst, W., and Hovenier, J. W.: First lidar observations of mesospheric hydroxyl, Geophys. Res. Lett., 25, 51-54, 1998.

Chane Ming, F., Vignelles, D., Jegou, F., Berthet, G., Renard, J.-B., Gheusi, F., and Kuleshov, Y.: Gravity-wave effects on tracer gases and stratospheric aerosol concentrations during the 2013 ChArMEx campaign, Atmos. Chem. Phys., 16, 8023-8042, https://doi.org/10.5194/acp-16-8023-2016, 2016.

Damiani, A., Storini, M., Santee, M. L., and Wang, S.: Variability of the nighttime OH layer and mesospheric ozone at high latitudes during northern winter: influence of meteorology, Atmos. Chem. Phys., 10, 10291-10303, doi:10.5194/acp-10-10291-2010, 2010.

Eckermann, S. D., Gibson-Wilde, D. E., and Bacmeister, J. T.: Gravity Wave Perturbations of Minor Constituents: A Parcel Advection Methodology, J. Atmos. Sci., 55, 3521–3539, 1998.

Eriksson P.: Microwave radiometric observations of the middle atmosphere: simulations and inversions. Ph.D. thesis, Chalmers University of Technology, 1999.

Eriksson, P., Jimenez, C., and Buehler, S. A.: Qpack, a general tool for instrument simulation and retrieval work, JQSRT, 91(1), 47-64, 2005.

Eriksson, P., Buehler, S. A., Davis, C. P., Emde, C., and Lemke, O.: ARTS, the atmospheric radiative transfer simulator, Version 2. JQSRT, 112, 1551-1558, 2011.

Forkman, P., Eriksson, P., and Murtagh, D.: Observing the vertical branch of the mesospheric circulation at lat N60˚ using ground based measurements of CO and H2O, J. Geophys. Res., 110, 107, doi:10.1029/2004JD004916, 2005.

Forkman, P., Christensen, O. M., Eriksson, P., Urban, J., and Funke, B.: Six years of mesospheric CO estimated from ground-based frequency-switched microwave radiometry at 57° N compared with satellite instruments, Atmos. Meas. Tech., 5, 2827–2841, doi:10.5194/amt-5-2827-2012, 2012.

Fritts, D. C., and Alexander, M., J.: Gravity wave dynamics and effects in the middle atmosphere, Rev. Geophys., 41, 1003, doi:10.1029/2001RG000106, 2003.

Janssen M.A.: Atmospheric remote sensing by microwave radiometry, Wiley, New York, 37-90, 1993.

Garcia, R. R. and Solomon, S.: A Numerical Model of the Zonally Averaged Dynamical and Chemical Structure of the Middle Atmosphere, J. Geophys. Res., 88, 1379–1400, doi:10.1029/JC088iC02p01379, 1983.

Garcia, R., Marsh, D., Kinnison, D., Boville, B., and Sassi, F.: Simulation of secular trends in the middle atmosphere, 1950-2003, J. Geophys. Res., 112, D09301, doi:10.1029/2006JD007485, 2007.

Garcia, R. R., López-Puertas M., Funke D., Marsh D. R., Kinnison D. E., Smith A. K., and González-Galindo F.: On the distribution of CO2 and CO in the mesosphere and lower thermosphere, J. Geophys. Res., 119, 5700–5718, doi:10.1002/2013JD021208, 2014.

Hocke, K., Kämpfer, N, Feist, D. G., Calisesi, Y., Jiang, J. H., and Chabrillat, S.: Temporal variance of lower mesospheric ozone over Switzerland during winter 2000/2001, Geophys. Res. Lett., 33, L09801, doi:10.1029/2005GL025496, 2006.

Hoffmann, C. G., Raffalski, U., Palm, M., Funke, B., Golchert, S. H. W., Hochschild, G., and Notholt, J.: Observation of stratomesospheric CO above Kiruna with ground-based microwave radiometry – retrieval and satellite comparison, Atmos. Meas. Tech., 4, 2389–2408, doi:10.5194/amt-4-2389-2011, 2011.

Hoffmann, C. G.: Application of CO as a tracer for dynamics in the polar winter middle atmosphere, Ph.D. thesis, Institut für Umweltphysik, Universität Bremen, Germany, 142 pp., 2012.

Lee, J. N., Wu, D. L., Manney, G. L., Schwartz, M. J., Lambert, A., Livesey, N. J., Minschwaner, K. R., Pumphrey, H. C., and Read, W. G.: Aura Microwave Limb Sounder observations of the polar middle atmosphere: Dynamics and transport of CO and H2O, J. Geophys. Res., 116, D05110, doi:10.1029/2010JD014608, 2011.

Livesey, N. J., Read, W. G., Wagner, P. A., Froidevaux, L., Lambert, A., Manney, G. L., Millán Valle, L. F., Pumphrey, H. C., Santee, M. L., Schwartz, M. J., Wang, S., Fuller, R. A., Jarnot, R. F., Knosp, B. W., and Martinez, E.: Version 4.2x Level 2 data quality and description document, Tech. rep., Jet Propulsion Laboratory, 2015.

Manney, G. L., Schwartz, M. J., Krüger, K., Santee, M. L., Pawson, S., Lee, J. N., Daffer, W. H., Fuller, R. A., and Livesey, N. J.: Aura Microwave Limb Sounder observations of dynamics and transport during the record-breaking 2009 Arctic stratospheric major warming, Geophys. Res. Lett., 36, L12815, doi:10.1029/2009GL038586, 2009.

Manney, G. L., Lawrence, Z. D., Santee, M. L., Read, W. G., Livesey, N. J., Lambert, A., Froidevaux, L., Pumphrey, H. C., and Schwartz, M. J.: A minor sudden stratospheric warming with a major impact: Transport and polar processing in the 2014/2015 Arctic winter, Geophys. Res. Lett., 42, 7808–7816, doi:10.1002/2015GL065864, 2015.

Marquardt, D.: An algorithm for least squares estimation on nonlinear parameters, J. Soc. Ind. Appl. Math., 11, 431–41, 1963.

Nassar, R., Bernath, P. F., Boone, C. D., Manney, G. L., McLeod, S. D., Rinsland, C. P., Skelton, R., and Walker, K. A.: ACE-FTS measurements across the edge of the winter 2004 Arctic vortex, Geophys. Res. Lett., 32, L15S05, doi:10.1029/2005GL022671, 2005.

Noguchi, K., Imamura, T., Oyama, K. -I., and Bodeker, G. E: A global statistical study on the origin of small-scale ozone vertical structures in the lower stratosphere, J. Geophys. Res., 111, D23105, doi:10.1029/2006JD007232, 2006.

Parrish, A., de Zafra, R. L., Solomon, P. M., and Barrett, J. W.: A ground-based technique for millimeter wave spectroscopic observations of stratospheric trace constituents, Radio Sci., 23, 106–118, 1988.

Picone, J.M., Hedin, A.E., Drob, D.P., and Aikin, A.C.: NRL-MSISE-00 Empirical Model of the Atmosphere: Statistical Comparisons and Scientific Issues, J. Geophys. Res., doi:10.1029/2002JA009430, 2002.

Raffalski, U., Hochschild, G., Kopp, G., and Urban, J.: Evolution of stratospheric ozone during winter 2002/2003 as observed by a ground-based millimetre wave radiometer at Kiruna, Sweden, Atmos. Chem. Phys., 5, 1399–1407, doi:10.5194/acp-5-1399-2005, 2005.

Rodgers, C. D. and Connor, B. J.: Intercomparison of remote sounding instruments, J. Geophys. Res., 108, 4116, doi:10.1029/2002JD002299, 2003.

Rodgers, C. D.: Inverse methods for atmospheric remote sounding: Theory and practice. Vol 2. Series on atmospheric and ocean physics. Singapore: World Scientific, 2000.

Rosenkranz, P.W.:Water vapor microwave continuum absorption: A comparison of measurements and models, Radio Science, 33, 919–928, 1998.

Rosenkranz, P.W.: Absorption of microwaves by atmospheric gases, in: Janssen M.A.: Atmospheric remote sensing by microwave radiometry, Wiley, New York, 37-90, 1993.

Rothman, L. S., Gordon, I. E., Barbe, A., Chris Benner, D., Bernath, P. F., Birk, M., Boudon, V., Brown, L. R., Campargue, A., Champion, J. –P., Chance, K., Couderti, L. H., Dana, V., Devi, V. M., Fally, S.,Flaud, J. –M., Gamache, R. R., Goldman, A., Jacquemart, D., Kleiner, I., Lacome, N., Lafferty, W. J., Mandin, J. –Y., Massie, S. T., Mikhailenko, S. N., Miller, C. E., Moazzen-Ahmadi, N., Naumenko, O. V., Nikitin, A. V., Orphal, J., Perevalov, V. I., Perrin, A., Predoi-Cross, A., Rinsland, C. P., Rotger, M., Simeckova, M., Smith M. A. H., Sung K., Tashkun, S. A., Tennyson, J., Toth, R. A., Vandaele, A. C., and Vander Auwera, J.: The HITRAN 2008 molecular spectroscopic database, J. Quant. Spec. Rad. Trans., 110(9-10), 533-572, 2009.

Ryan, N. J., and Walker, K. A.: The effect of spectroscopic parameter inaccuracies on ground-based millimeter wave remote sensing of the atmosphere. JQSRT, 161, 50-59, doi:10.1016/j.jqsrt.2015.03.012, 2015.

Ryan, N. J., Palm, M., Raffalski, U., Larsson, R., Manney, G., Millán, L., and Notholt, J.: Strato-mesospheric carbon monoxide profiles above Kiruna, Sweden (67.8 ° N, 20.4 ° E), since 2008, Earth Syst. Sci. Data, 9, 77-89, doi:10.5194/essd-9-77-2017, 2017.

Ryan, N. J., Kinnison, D. E., Garcia, R. R., Hoffmann, C. G., Palm, M., Raffalski, U., and Notholt, J.: Assessing the ability to derive rates of polar middle-atmospheric descent using trace gas measurements from remote sensors, Atmos. Chem. Phys., 18, 1457-1474, https://doi.org/10.5194/acp-18-1457-2018, 2018.

Schranz, F., Fernandez, S., Kämpfer, N., and Palm, M.: Diurnal variation in middle-atmospheric ozone observed by ground-based microwave radiometry at Ny-Ålesund over 1 year, Atmos. Chem. Phys., 18, 4113-4130, https://doi.org/10.5194/acp-18-4113-2018, 2018.

Schranz, F., Tschanz, B., Rüfenacht, R., Hocke, K., Palm, M., and Kämpfer, N.: Investigation of Arctic middle-atmospheric dynamics using 3 years of H2O and O3 measurements from microwave radiometers at Ny-Ålesund, Atmos. Chem. Phys. Discuss., https://doi.org/10.5194/acp-2018-1299, in review, 2019.

Schwartz, M., Pumphrey, H., Livesey, N. and Read, W.: MLS/Aura Level 2 Carbon Monoxide (CO) Mixing Ratio V004, version 004, Greenbelt, MD, USA, Goddard Earth Sciences Data and Information Services Center (GES DISC), Accessed June 2018 at 10.5067/AURA/MLS/DATA2005.

Smith, A. K., Garcia, R. R., Marsh, D. R., and Richter J. H.: WACCM simulations of the mean circulation and trace species transport in the winter mesosphere, J. Geophys. Res., 116, D20115, doi:10.1029/2011JD016083, 2011.

Solomon, S., Garcia, R. R., Olivero, J. G., Bevilacqua, R. M., Schwarzt, P. R., Clancy, R. T., and Muhleman, D. O.: Photochemistry and Transport of Carbon Monoxide in the Middle Atmosphere, J. Atmos. Sci., 42(10), 1072-1083, 1985.

Stanimirovic, S., Altschuler, D., Goldsmith, P., Salter, C.:Single-Dish Radio Astronomy: Techniques and Applications, ASP Conf. Ser., vol. 278, 2002.

Straub, C., Tschanz, B., Hocke, K., Kämpfer, N., and Smith, A. K.: Transport of mesospheric H2O during and after the stratospheric sudden warming of January 2010: observation and simulation, Atmos. Chem. Phys., 12, 5413–5427, doi:10.5194/acp-12-54132012, 2012.

Straub, C., Espy, P., Hibbins, R. E., and Newnham, D. A.: Mesospheric CO above Troll station, Antarctica observed by a ground based microwave radiometer. Earth Syst. Sci. Data, 5, 199–208, doi:10.5194/essd-5-199-2013, 2013.

Studer, S., Hocke, K., Schanz, A., Schmidt, H., and Kämpfer, N.: A climatology of the diurnal variations in stratospheric and mesospheric ozone over Bern, Switzerland, Atmos. Chem. Phys., 14, 5905-5919, https://doi.org/10.5194/acp-14-5905-2014, 2014.

Waters, J., Froidevaux, L., Harwood, R., Jarno, R., Pickett, H., Read, W., Siegel, P., Cofield, R., Filipiak, M., Flower, D., Holden, J., Lau, G., Livesey, N., Manney, G., Pumphrey, H., Santee, M., Wu, D., Cuddy, D., Lay, R., Loo, M., Perun, V., Schwartz, M., Stek, P., Thurstans, R., Boyles, M., Chandra, S., Chavez, M., Chen, G.-S., Chudasama, B., Dodge, R., Fuller, R., Girard, M., Jiang, J., Jiang, Y., Knosp, B., LaBelle, R., Lam, J., Lee, K., Miller, D., Oswald, J., Patel, N., Pukala, D., Quintero, O., Scaff, D., Snyder, W., Tope, M., Wagner, P., and Walch, M.: The Earth Observing System Microwave Limb Sounder (EOSMLS) on the Aura satellite, IEEE T. Geosci. Remote, 44, 1075–1092, 2006.

Zhu, X., and J. R. Holton, J., R.: Mean fields induced by local gravity-wave forcing in the middle atmosphere, J. Atmos. Sci., 44, 620–630, 1987.

Atmos. Meas. Tech. Discuss., https://doi.org/10.5194/amt-2019-121
Manuscript under review for journal Atmos. Meas. Tech.
Discussion started: 28 March 2019

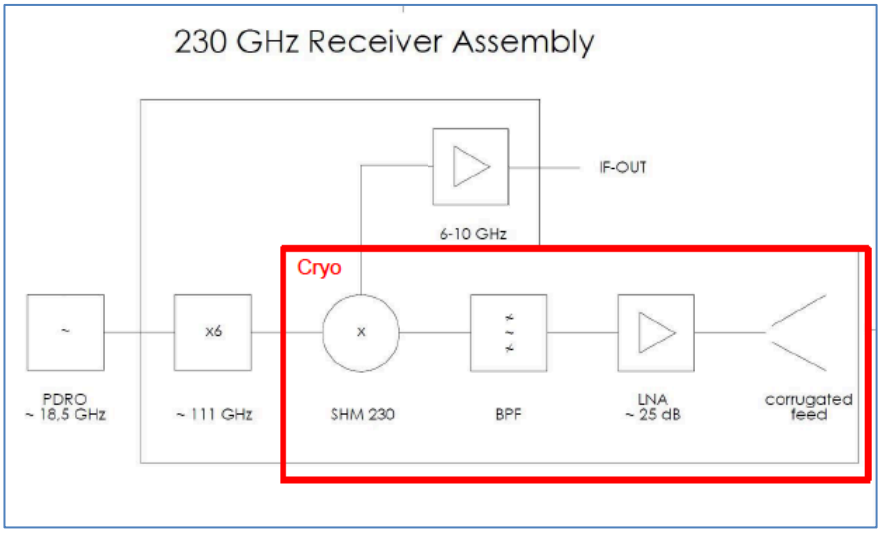

Figure 1: Schematic of the CORAM receiver. The atmospheric signal passes through the quasioptical system (not shown) and a window in the cryocooler before reaching (in order) a corrugated feed horn, a 230 GHz LNA, a waveguide filter (BPF), and a sub-harmonic mixer (SHM), where the signal is downconverted to an intermediate frequency (IF) of 8.5 GHz. The IF signal exits the cryocooler and passes through a room temperature LNA. The atmospheric signal is mixed at the SHM with a local oscillator signal, which is an 18.5 GHz signal from a phase-locked dielectric resonator oscillator (PDRO) that is passed through a X6 frequency multiplier, to provide 111 GHz at the SHM.

Atmos. Meas. Tech. Discuss., https://doi.org/10.5194/amt-2019-121
Manuscript under review for journal Atmos. Meas. Tech.
Discussion started: 28 March 2019

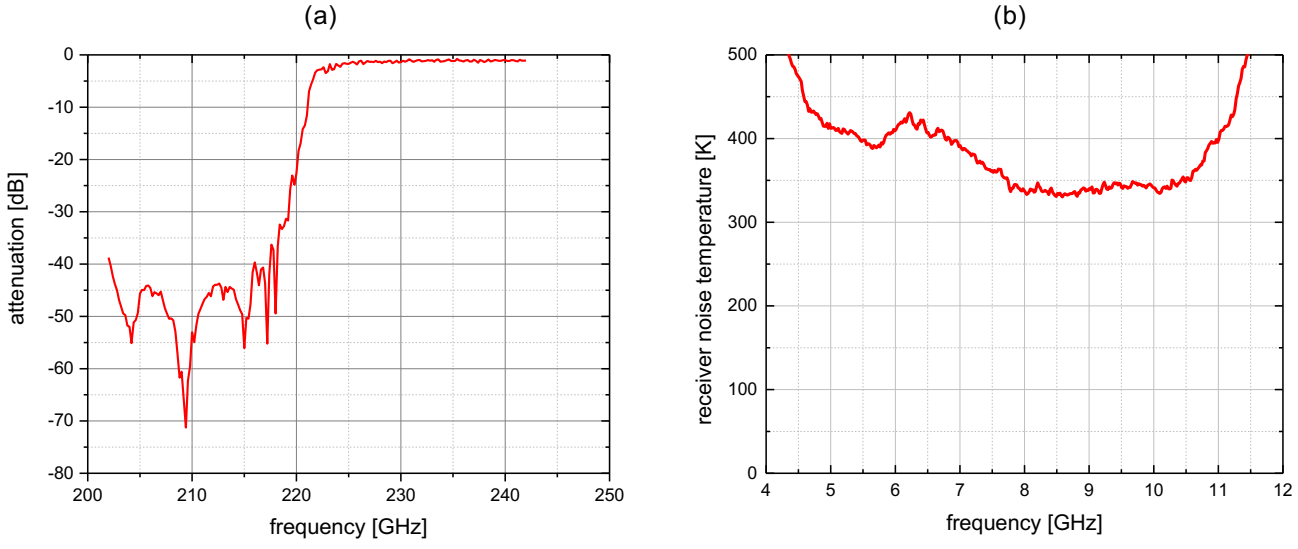

Figure 2: (a) The frequency response of the waveguide filter (BPF in Fig. 1) in used in CORAM to supress the unwanted sideband signal at 213.5 GHz. (b) The receiver noise temperature for CORAM after downconversion to 8.5 GHz. This measurement is made after the first room temperature LNA (Fig. 1) and before the second downconversion to 1.5 GHz. The cryocooler components are at 39 K. The single sideband system noise temperature for CORAM is ~ 600 K (Sect. 2.1).

Atmos. Meas. Tech. Discuss., https://doi.org/10.5194/amt-2019-121
Manuscript under review for journal Atmos. Meas. Tech.
Discussion started: 28 March 2019

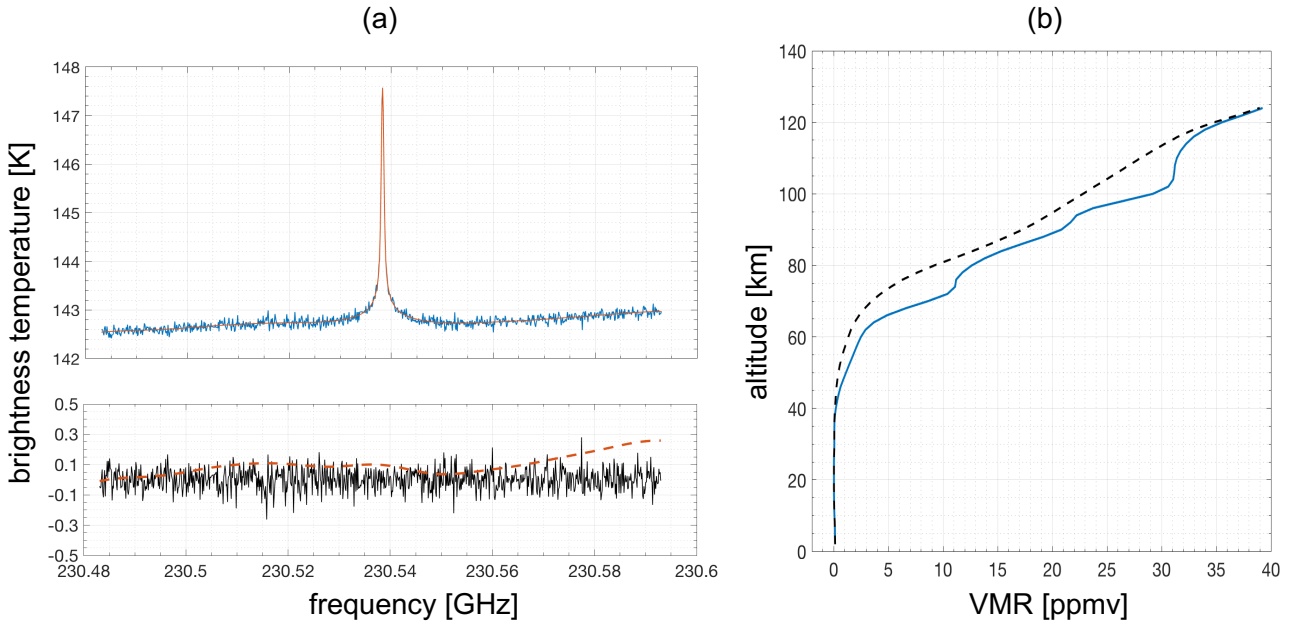

Figure 3: (a) Upper: an example spectrum measured by CORAM on Dec 24th 2017 between 20:04 and 21:03 UTC. The inversion fit to the measurement is shown (smoother red line). Lower: the residual of the measurement and the inversion fit (solid black line). The dashed red line shows the baseline fit for the inversion, which is part of the inversion fit (Sect. 2.2). (b) The CO profile retrieved from the measurement (solid blue) and the a priori profile that is used as input to the inversion (dashed black).

Atmos. Meas. Tech. Discuss., https://doi.org/10.5194/amt-2019-121
Manuscript under review for journal Atmos. Meas. Tech.
Discussion started: 28 March 2019

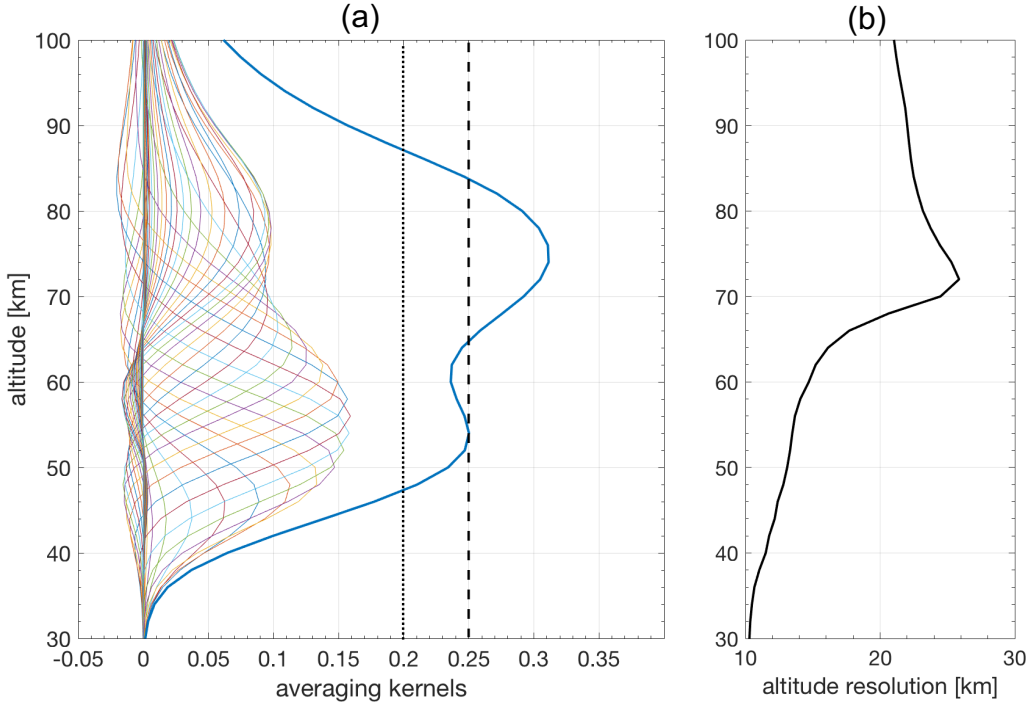

Figure 4: The mean averaging kernels for the CORAM inversions. The measurement response (sum of the rows of the averaging kernels) divided by 4 is shown in solid blue. The dashed black line and the dotted black line indicate a measurement response of 1.0 and 0.8, respectively. (b) The mean altitude resolution of the CORAM CO profiles, calculated from the FWHM of the averaging kernels.

Atmos. Meas. Tech. Discuss., https://doi.org/10.5194/amt-2019-121
Manuscript under review for journal Atmos. Meas. Tech.
Discussion started: 28 March 2019

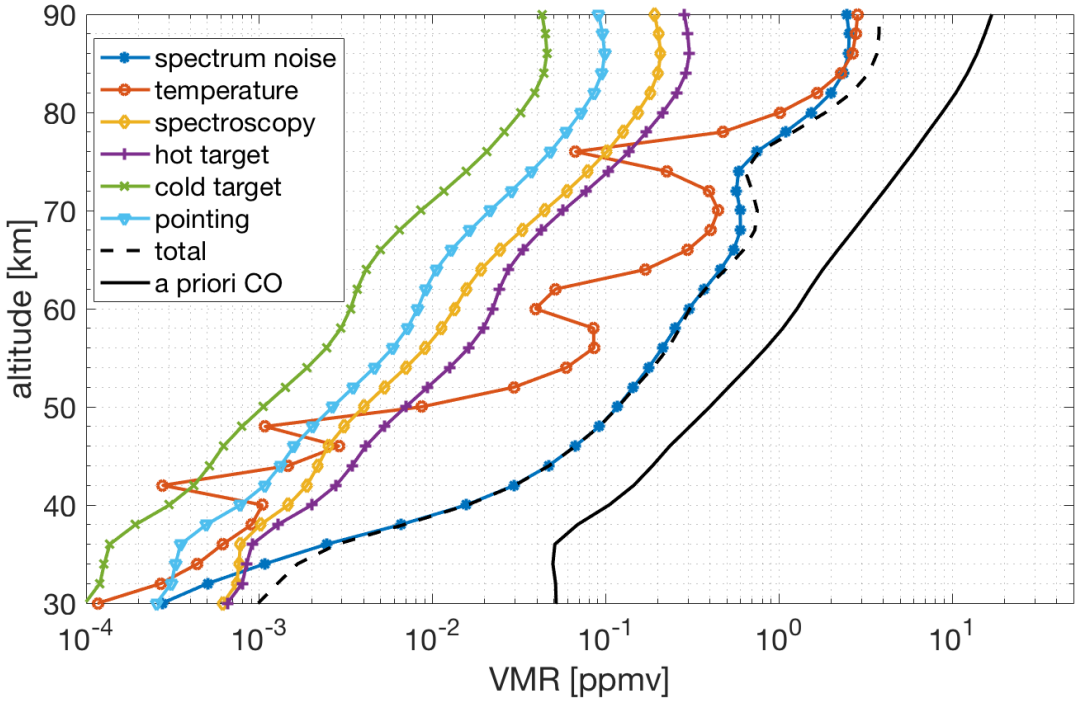

Figure 5: The estimated error contributions to the CORAM CO profiles. The spectrum noise is calculated as an average of the noise on all CORAM measurements, and the other estimates are calculated through perturbations about the a priori CO profile (Sect. 2.4).

Atmos. Meas. Tech. Discuss., https://doi.org/10.5194/amt-2019-121
Manuscript under review for journal Atmos. Meas. Tech.
Discussion started: 28 March 2019

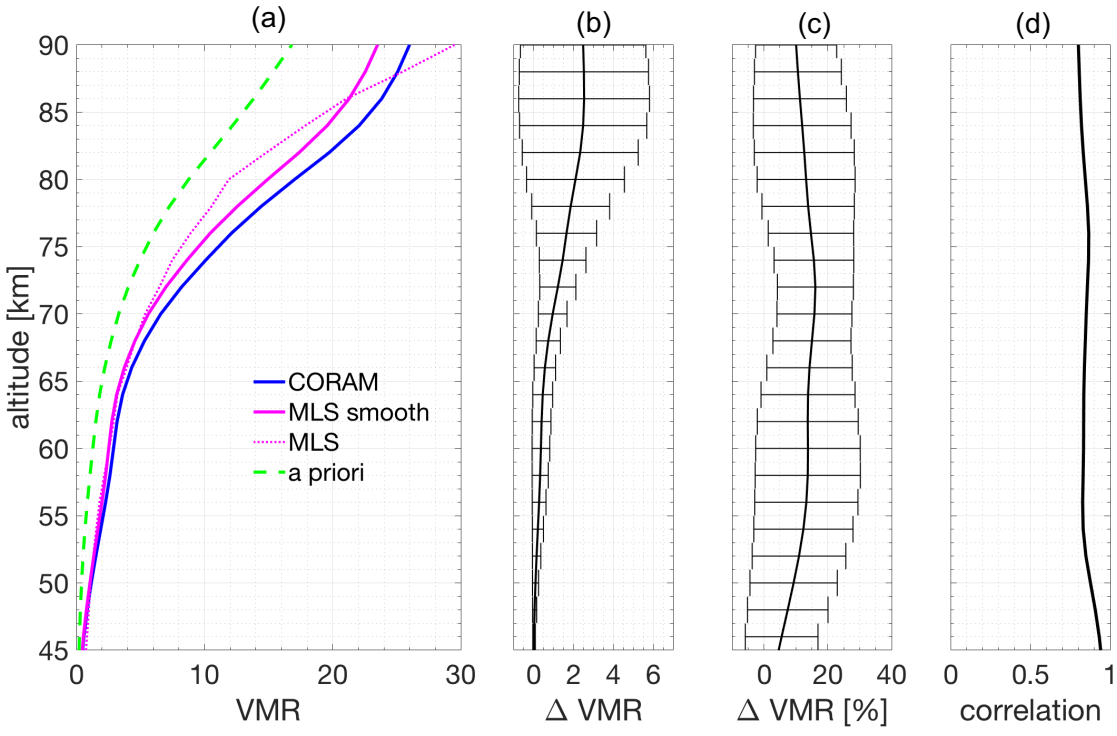

Figure 6: (a) The mean of the daily CORAM and MLS CO profiles above Ny-Ålesund. The mean of the unsmoothed MLS profiles is also shown as well as the a prioiri profile used for the CORAM inversions. (b) The absolute difference of the mean CORAM and smoothed MLS profiles, with the standard deviation of the differences as the whiskers on the line. (c) The same as for (b) but with the difference as a percentage of the mean CORAM and MLS profiles. (d) The correlation coefficients of the CORAM and smoothed MLS data.

Atmos. Meas. Tech. Discuss., https://doi.org/10.5194/amt-2019-121
Manuscript under review for journal Atmos. Meas. Tech.
Discussion started: 28 March 2019

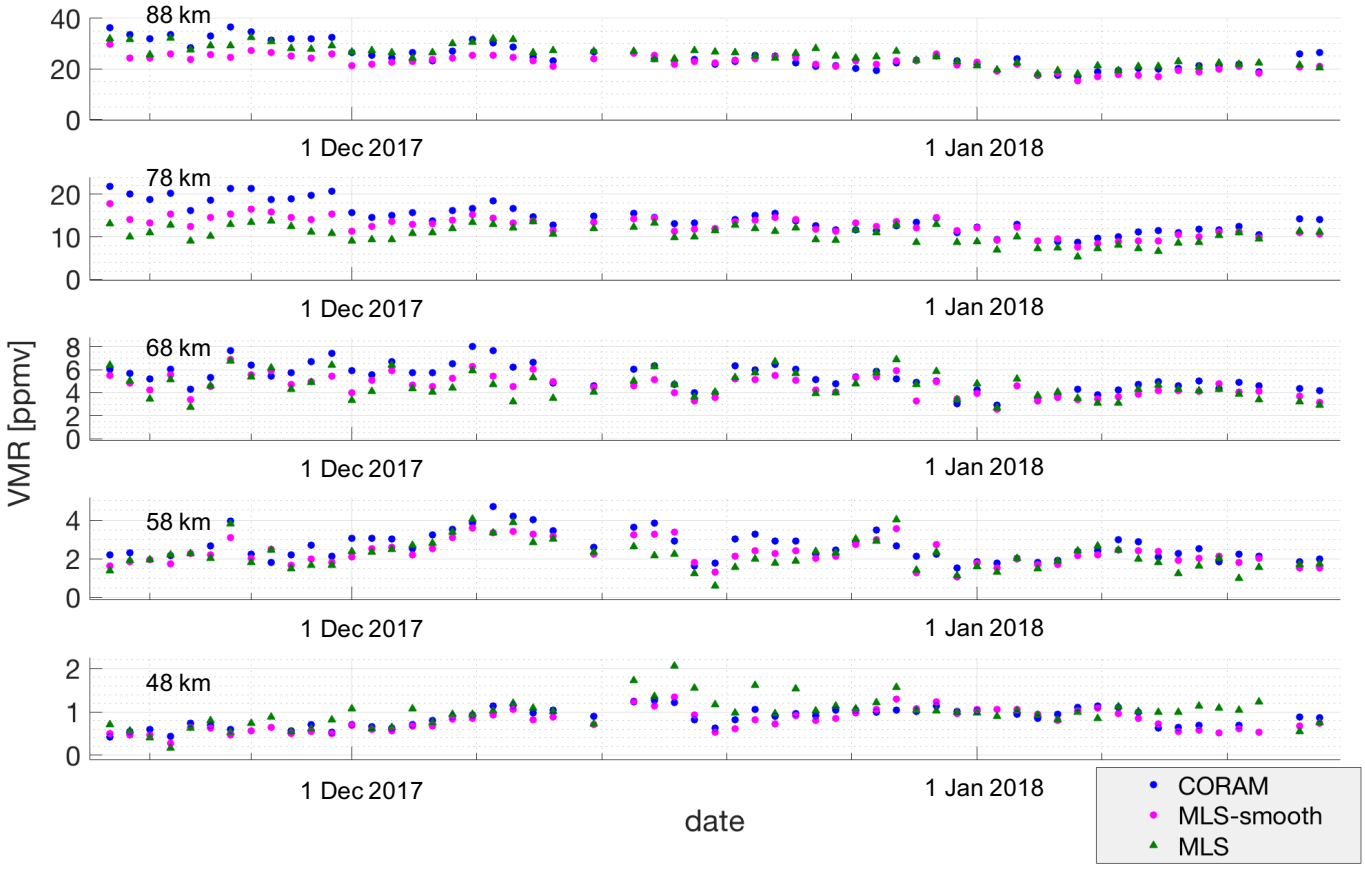

Figure 7: Time series of the daily CORAM and MLS CO profiles.

Atmos. Meas. Tech. Discuss., https://doi.org/10.5194/amt-2019-121
Manuscript under review for journal Atmos. Meas. Tech.
Discussion started: 28 March 2019

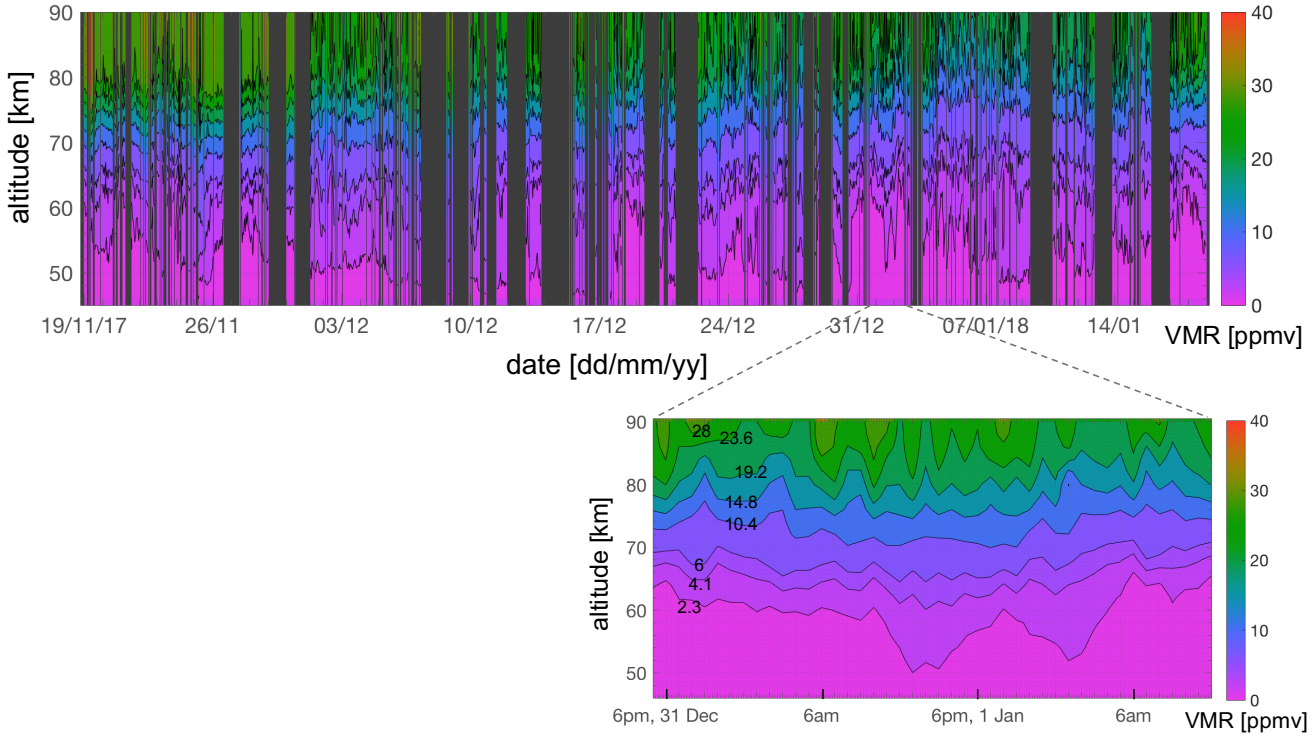

Figure 8: CORAM CO profiles at 1 hr resolution from mid-November 2017 to mid-January 2018. Blank areas are gaps in the data record. The zoomed-in plot shows measurements over a 42-hour period beginning at 6pm on December 31st 2017. The contours are non-uniformly spaced between 0.4 and 28 ppmv, and filled to ease readability. The Isoluminant colour map from Kindlmann et al. (2002) is used. Contour values are [0.4, 2.3, 4.1, 6.0, 10.4, 14.8, 19.2, 23.6, 28.0].